High-resolution electron-energy-loss study of the surfaces and energy gaps of cleaved high-temperature superconductors

B. N. J. Persson
Institut für Festkörperforschung der Forschungsanlage Jülich, D-5170 Jülich, West Germany and IBM Research Division, Zürich Research Laboratory, 8803 Rüschlikon, Switzerland

J. E. Demuth
IBM Research Division, T. J. Watson Research Center, Yorktown Heights, New York 10598
(Received 4 January 1990)

High-resolution electron-energy-loss spectroscopy (HREELS) is used to characterize the resistivity, vibrational, and electronic structure of $YBa_2Cu_3O_7$, $Bi_2Sr_2CaCu_2O_8$, and TiS_2 single crystals cleaved in ultrahigh vacuum. The HREELS data are analyzed using dipole-scattering theory for a semi-infinite sequence of conducting sheets separated by dielectric slabs. Cleaved surfaces show strong lateral inhomogeneities and a variety of terminations with different properties. Spectroscopy on superconducting regions for a variety of these Cu-O–based superconductors reveals an energy gap in the *ab* plane that corresponds to $(7.8\pm0.3)k_BT_c$. The superconducting gap of the 1:2:3 material shows a non-BCS temperature dependence. We also analyze the infrared reflection data from the 1:2:3 material obtained by different groups and find good agreement with our HREELS results. Based on these experimental results, we suggest that the transition to superconductivity is due to a Bose-Einstein condensation of the preexisting or "real" space pairs.

I. INTRODUCTION

The value of the energy gap in the Cu-O–based superconductors[1] is widely disputed but of fundamental importance. The short coherence length in the superconducting state in these materials may result in different surface and bulk properties. In particular, a different gap at the surface, or even a nonsuperconducting surface could arise that would be preferentially detected by many surface-sensitive methods such as tunneling[2] or photoemission.[3–5] Bulk measurements, on the other hand, such as infrared reflection-absorption spectroscopy (IRAS)[6–8] have proved to be difficult to interpret and controversial amongst different groups. This can arise from differences in samples as well as the fact that at low frequencies IRAS measures small variations away from the nearly unit reflectivity characteristic of a good conductor. As we will show later, the ir results are in general agreement with one another, albeit different interpretations.

In contrast to IRAS, loss measurements can probe gap excitations away from the strong elastically reflected peak. Recent Raman measurements[9] show a broad continuum which appears to be associated with superconductivity. Again, the low sensitivity of Raman usually requires studies of specularly smooth samples to minimize stray scattering and obtain good signal-to-noise ratios.

High-resolution electron-energy-loss spectroscopy[10] (HREELS) provides an important complement to both IRAS and Raman measurements as it has higher sensitivity and can be performed in a spot-focused mode so as to study the homogeneity of these surfaces. Both vibrational and electronic transitions can be monitored in addition to determining the frequency-dependent resistivity. Given the momentum associated with electrons, an $\sim 10^3$ wider range of k space can be accessed with HREELS than by optical methods. Also, angle-dependent, i.e., k-dependent, loss measurements are possible with electron scattering. We note here that HREELS has been used earlier to study the conductivity properties of metal surfaces[11] and of thin metallic films on semiconductor surfaces.[12] The high accuracy of this method is revealed in the study of Cu(100) (Ref. 11) where more detailed information about the low-frequency nonlocal optical response of this metal surface was achieved than previously possible.

Given the macroscopically measured bulk resistivity[13] of these Cu-O–based superconductors, we expect HREELS to be sensitive to several Cu-O layers thereby providing a comparable penetration depth as photoemission. Further, the interaction distance of the incident electron along the surface is ~ 1000 Å, which sets a lateral length scale (effectively a coherence length) to the properties one probes. Considering the complexity of these layered materials, one would not be surprised to find variations between such a "microscopic" HREELS determination of the resistivity and other macroscopic measurements of the resistivity.

A few HREELS studies[14–16] have already been performed on these new oxide superconductors. An early study of Fukuda *et al.*[14] of ceramic 1:2:3 samples at room temperature has shown an interesting broad feature at 60 meV for both superconducting and nonsuperconducting materials as well as a very high-loss background. Another study by Jacobi *et al.*[15] of a ceramic 1:2:3 sample performed with higher resolution revealed a similar 60-meV feature which was temperature independent. The high-

loss background also observed here was found to show a strong temperature dependence. While both these studies reveal interesting new features, the lack of dipole scattering conditions for ceramic samples precludes a rigorous interpretation of these results. Recent specular (dipole) scattering HREELS measurements by Kelly *et al.*[16] on single-crystal samples found strong sample-to-sample variations in the spectra and some evidence for a dipole-active mode near 50 meV.

Our HREELS studies discussed here and briefly reported earlier[17] reveal that such variations and certain loss features can be associated with different cleavage terminations as well as sample inhomogeneities. Thus, we believe that these earlier HREELS studies are limited due to such inhomogeneities, especially for the ceramic samples. The amount of exposed cleaved surface that we find to be superconducting correlates well to the width of the bulk superconducting transition and thereby the bulk homogeneity. Any surface inhomogeneities formed or exposed during cleavage are also important for other surface measurements such as photoemission where, for example, one wishes to probe the electronic structure of this intrinsic superconductor. In this work, we have not only characterized the different terminal surfaces but have studied the superconducting regions of both $YBa_2Cu_3O_7$ and $Bi_2Sr_2CaCu_2O_8$. Hereafter we will refer to these materials as 1:2:3 and 2:2:1:2, respectively.

Our studies reveal a large superconducting energy gap $\sim 8k_BT_c$ for both 1:2:3 and 2:2:1:2 thereby confirming the ir work by Schlesinger and Collins *et al.*[6] on the gap of 1:2:3. In addition, we determine the temperature dependence of the gap by HREELS and find that it exhibits non-BCS behavior. Being able to detect superconductivity directly with HREELS, we have also found that the superconducting nature of these surfaces are particularly susceptible to degradation with time or exposure to the electron beam. The latter is particularly important for a wide variety of electron spectroscopic measurements where low-energy electrons are directly involved or generated. In the following, we discuss the experimental problems and complexities of performing measurements on cleaved surfaces of this material (Sec. II), the theory needed to interpret much of these results (Sec. III), and finally the experimental results for 1:2:3 and 2:2:1:2 surfaces (Sec. IV). We also show results for another layered material, TiS_2, which also exhibit some similar and unexpected layer-dependent properties.

II. EXPERIMENT

HREELS measurements were performed in an ultrahigh vacuum (UHV) system at a background pressure of 6×10^{-11} Torr without sample cooling and at a background pressure of $<2\times10^{-11}$ Torr with He sample cooling. This chamber houses our single-pass 2.5-cm-diam hemispherical analyzer-based electron-energy-loss spectrometer which has a fixed total scattering angle of 90°. For this work the analyzer was initially operated with a conventional pass energy of ~ 0.5 eV and an acceptance angle of $\sim 2.5°$. The nature of these samples, however, required ultimate pass energies of ~ 100 meV and acceptance angles of 1.1–1.6° to achieve satisfactory results. These small pass energies and angular acceptances were needed to probe isolated crystalline regions and reduce any spurious signals arising from the sample and/or the spectrometer. Many of the 2:2:1:2 samples, particularly the larger ones ($\sim 1\times1.5$ mm^2), have 0.5°–1.5° variations in crystal orientations which can introduce or superimpose suprious features in the loss spectra. Figure 1(a) shows the result of an early HREELS measurement where the electron beam happened to overlap two tilted regions of a 2:2:1:2 crystal so as to produce two elastic peaks in the spectrum. From the peak splitting observed we estimate a tilt of 0.25°–0.5° in the two crystallites. For this reason small 2:2:1:2 crystals ($\sim 0.5\times1$ mm^2) were selected for study even though larger samples were available.

The spot focusing of our hemispherical analyzer system was found to produce an ~ 50-μm-diam beam as determined by laterally scanning the beam over irregular regions of the sample as shown in Fig. 1(b). This beam profile incident on our 45° inclined sample probes a $\sim 50\times70$-μm^2 elliptical area on our sample. Such spot focusing also proved crucial in these studies as it has allowed us to study small flat regions of these surfaces as well as identify surface inhomogeneities. In general, such inhomogeneities and/or mosaic structures in high-T_c samples will limit HREELS studies until higher quality, larger, single crystals of these materials are generally available.

The single-crystal 1:2:3 samples were grown by Holtzberg and Feilds from the pseudoternary BaO-CuO-Y_2O_3 system and post annealed in O_2 at 420 °C for 10 d.[18] The samples exhibited T_c's of 93 K with a 10–90 % transition width (ΔT) of 0.3 K. All the data obtained here for 1:2:3 samples were from twinned crystals. The 2:2:1:2

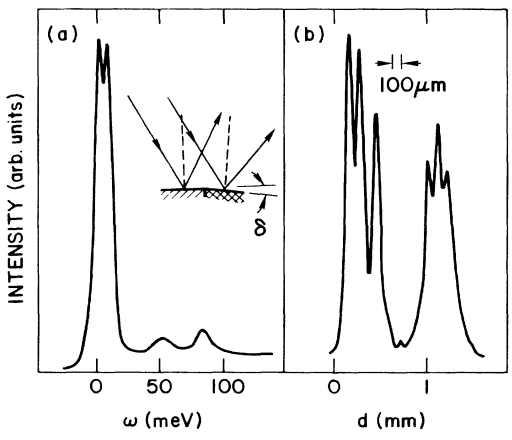

FIG. 1. Electron-energy-loss spectroscopy form a 0.5×1.5 mm^2 2:2:1:2 single crystal cleaved in ultrahigh vacuum using a 2° acceptance angle. The electron beam covers two small, flat, but tilted, "domains" resulting in two specular beams and two elastic peaks in HREEL spectra. In (b) the variations in elastic peak intensity as a function of position along the samples are shown which are also associated with such domains.

samples were grown by Chandrashekhar from polycrystalline $Bi_{4.4}Sr_3Ca_3Cu_{3.64}O_x$ maintained at 875 °C in a Pt crucible for about 40–50 h.[19] Typical 2:2:1:2 samples had T_c's of 85 K and $\Delta T = 3$ K, with some samples having T_c's of 75 or 91 K. Microprobe analysis reveals that the 1:2:3 samples are essentially stochiometric but that the 2:2:1:2 superconducting samples were not. The chemical formula for the typical superconducting 2:2:1:2 sample was $Bi_{2.2}Sr_{1.8}CaCu_2O_{8.15}$.

Crystals of each material were selected from several batches based on their overall uniformity and ac susceptibility measurements of T_c. Interestingly, post analysis of cleaved 2:2:1:2 samples in many cases revealed strong variations in T_c from that of the starting samples. Since the ac susceptibility measurement senses deep within the samples, such variations in T_c must be associated with bulk inhomogeneities within the sample. Optical microscopy of both *in situ* and *ex situ* cleaved 2:2:1:2 samples using polarized light also reveals strong lateral inhomogeneities. Examples of such micrographs for two samples are shown in Fig. 2. Here, some of the light and dark regions of the sample shown in Figs. 2(b)–2(e) are the result of polarization differences from different terminal layers. These polarizations also show a 90° rotation with respect to one another. The opposite sides of each of these cleaved samples [2(c) and 2(e)] do not always show the polarization that one expects from the other side. Micro-Raman as well as micro-Auger analysis performed under UHV on these different regions suggest no significant compositional differences—but do not rule out small oxygen variations. These cleavage irregularities, however, produce variations in the surface resistivity as discussed later. For 2:2:1:2 we associate these higher-resistivity (but still metallic) layers with cleavage at oxygen-rich layers arising at regions where switching of the *a* and *b* crystallographic directions occur. From these observations it appears that regions where the *a-b* directions switch are preferred locations for cleavage. In contrast, the 1:2:3 samples do not show similar effects but instead show the twinning structure. However, we do note a few cases of 1:2:3 cleavage that revealed small regions of a $BaCuO_2$ crystalline layer which has been readily identified by its different reflectivity in polarized light and subsequent micro-Raman analysis.

Overall, 12 thin samples of each crystal ($<1\times0.5$ mm^2) were mounted using conductive epoxy onto a copper coldfinger at the end of a rotatable tube containing an Air products cryotip. The sample temperature was measured from a chromel-alumel thermocouple inside the coldfinger which was later calibrated from another chromel-alumel thermocouple mounted near the sample. Cleavage was performed by pulling off a small metal tab *in vacuo* that was epoxied onto the top surface of the sample. Furthermore, epoxy near the sample edges could be detected and distinguished by its characteristic hydrocarbon vibrations.

The flatness of the cleaved samples is another important issue which limits the cleavage quality and our abili-

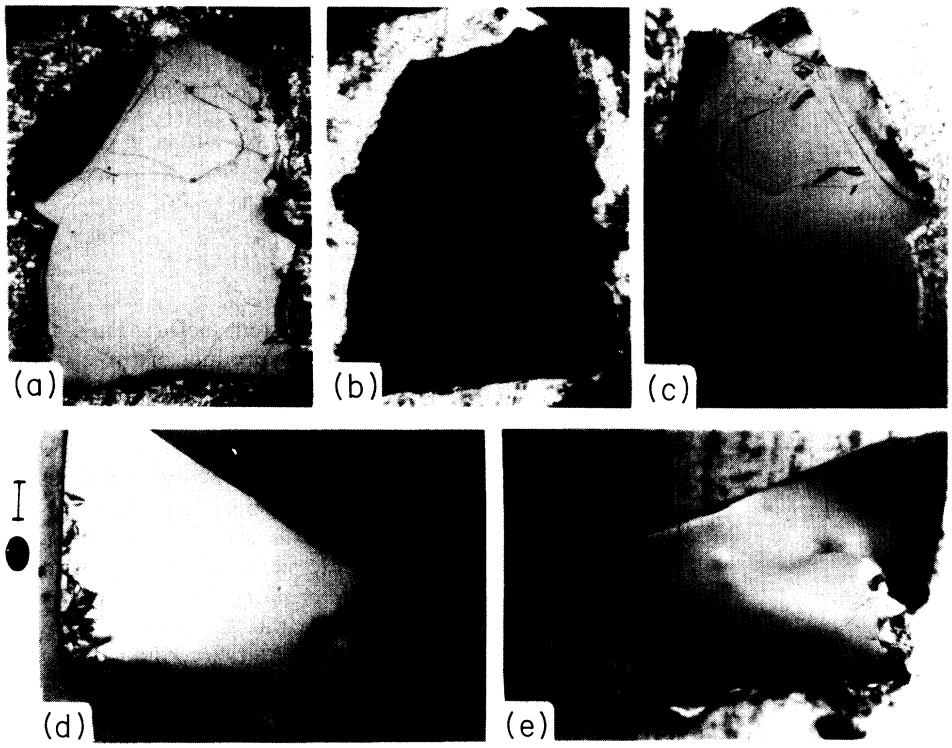

FIG. 2. Micrographs of 2:2:1:2 surfaces under (a) normal light and (b)–(e) polarized light. (b) and (c) and (d) and (e) reflect opposite cleavage pairs of the same sample cleaved in vacuum and in air, respectively. The bar alongside (d) corresponds to 100 μm with the ellipse indicating the beam profile on the sample.

ty to calibrate the acceptance angles of the spectrometer. The 2:2:1:2 samples as discussed earlier show no apparent differences between cleavage at 22 and 298 K. In contrast, the flattest and most uniform 1:2:3 sample occurred for cleavage at 298 K, whereas cleavage at 22 K produced large step densities and irregular glassy fracture regions. This, we believe, occurs from the external stress on the sample arising from differential contraction at low temperatures. We note that even on the best room-temperature cleaves some regions of the surface failed to show superconductivity whereas others did. Finally, angle-dependent measurements were also performed on a few of the flattest, most uniform, samples to verify that the loss features we discuss here arise from dipole scattering.

In general, since all the high-T_c samples were rather small, larger samples of both pyrolytic graphite (x-ray monochrometer grade) and TiS_2 were also mounted with the Cu-O samples and used to align and calibrate the spectrometer. We note that the angular spread of the graphite was larger than that of our high-T_c samples whereas the TiS_2 was much flatter than graphite and showed other interesting properties discussed later. The TiS_2 samples were grown by R. Figat using a standard vapor transport methods under HS_2-rich conditions. Chemical analysis of these samples reveals a composition of $TiS_{2.01}$ with x-ray analysis indicating a c axis of 5.6993 ± 0.0013 Å.

III. THEORY

The experimental data have been analyzed using the well-tested dipole-scattering theory.[20] Here the excitation process typically occurs when the incident electron is at a distance $d \sim v/\omega$ from the surface, where v is the velocity of the incident electrons and $\hbar\omega$ the loss energy. For incident electrons with a few electron volts kinetic energy and for the loss energies $\sim 10-100$ meV, one has $d \sim 10^2-10^3$ Å. The inelastic-scattered electrons form a narrow lobe close to the specular direction with an angular spread of $\Delta\theta \sim \hbar\omega/2E_0 \sim 0.1°-1°$. Since the acceptance angle of the spectrometer is of the order of 1°, most of these inelastically scattered electrons are detected.

Let us now briefly discuss the basic equations which are used in analyzing the HREELS data presented below. Let us first define the surface response function $g(q_\parallel,\omega)$ which plays an important role in what follows. Consider a semi-infinite medium occupying the half-space $z>0$. Let

$$\phi_{\rm ext}(\mathbf{x},t)=e^{i\mathbf{q}_\parallel\cdot\mathbf{x}_\parallel-q_\parallel z-i\omega t} \tag{1}$$

be an external potential which polarizes the medium. The induced-polarization charges will give rise to an induced potential which, for $z<0$ (i.e., outside the medium), can be written as

$$\phi_{\rm ind}(\mathbf{x},t)=-g(q_\parallel,\omega)e^{i\mathbf{q}_\parallel\cdot\mathbf{x}_\parallel+q_\parallel z-i\omega t} . \tag{2}$$

This equation defines $g(q_\parallel,\omega)$. It is implicitly assumed that the medium can be treated as translationally invariant parallel to the surface.

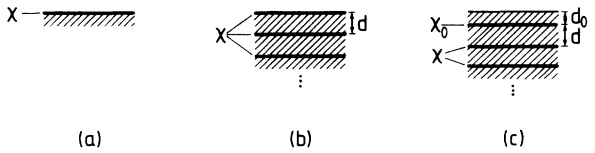

FIG. 3. Different models for layered compounds studied in this work: (a) a single conducting layer [treated as a two-dimensional electronic system characterized by the density-density correlation function $\chi(q,\omega)$] on a dielectric substrate; (b) an infinite sequence of conducting layers separated by dielectric slabs of thickness d; (c) the same as (b) but with a modified top layer consisting of a slab of thickness d_0 on top of a modified first conducting layer.

Now consider an electron with a few electron volts energy incident upon the surface. The electric field from the electron penetrates into the media where it can excite, e.g., electron-hole pairs, plasmons, or phonons. Let $\mathbf{k}$ and $\mathbf{k}'$ denote the wave vectors of the incident and inelastically scattered electron, respectively. Thus, $\hbar\mathbf{q}_\parallel=\hbar(\mathbf{k}_\parallel-\mathbf{k}'_\parallel)$ is the momentum transfer (parallel to the surface) to the excitation in the media and $\hbar\omega=\hbar^2(k^2-k'^2)/2m$ is the energy transfer. Let $P(k,k')d\Omega_{k'}d(\hbar\omega)$ be the probability that an incident electron is scattered inelastically into the range of energy losses between $\hbar\omega$ and $\hbar(\omega+d\omega)$ and into the solid angle $d\Omega_{k'}$ around the direction of $\mathbf{k}'$. For small momentum transfer, $q_\parallel \ll k$, one has[20,21]

$$P(k,k')=\frac{2}{(ea_0\pi)^2}\frac{1}{\cos\alpha}\frac{k'}{k}\frac{q_\parallel}{(q_\parallel^2+q_\perp^2)^2}\mathrm{Img}(q_\parallel,\omega)$$
$$\equiv A(k,k')\mathrm{Img}(q_\parallel,\omega) , \tag{3}$$

where $q_\perp=k_z-k'_z$, and α is the angle of incidence. At finite temperatures $P(k,k')$ is also multiplied by an additional term $(n_\omega+1)$ where

$$n_\omega=\frac{1}{e^{\hbar\omega/k_BT}-1}$$

is the Bose-Einstein factor. Thus, the inelastic-scattering probability is a product of three factors—$(n_\omega+1)$, a kinematic prefactor, and the surface-loss function. The kinematic prefactor $A(k,k')$ depends strongly on the loss energy $\hbar\omega$ ($A\sim\omega^{-3}$ as $\omega\to 0$) but is independent of the properties of the medium, whereas the loss function $\mathrm{Img}(q_\parallel,\omega)$ is proportional to the power absorption in the medium due to an external potential of the form (1). $g(q_\parallel,\omega)$ enters the inelastic-scattering probability (3) because it determines the induced electric field outside the substrate [via (2)]. It is this time-varying field that can scatter the incident electron inelastically.

Let us now consider a layered material where the conductivity within the planes is much higher than in the orthogonal direction.[22] We will need $g(q_\parallel,\omega)$ for the three cases illustrated in Fig. 3, i.e., (a) for a single conducting sheet on top of a dielectric medium, (b) for a semi-infinite sequence of conducting sheets separated by dielectric slabs of thickness d and (c) for a modified first layer on top of a layered material of the type shown in Fig. 2(b).

A. Top layer conducting sheet

This case could correspond, for example, to a thin metallic film on a semiconductor or an insulator (see Ref. 12 for such applications). The g function is[19]

$$g=1-\frac{2}{1+\epsilon-4\pi q_{\parallel}\sigma/i\omega} . \tag{4}$$

Here $\sigma(q_{\parallel},\omega)$ is the two-dimensional conductivity for a conducting sheet which can be related to the density-density correlation function $\chi(q_{\parallel},\omega)$ via $\chi=\sigma q_{\parallel}^2/i\omega$, and ϵ is the frequency-independent dielectric constant of the intervening layers. In the present work we assume the "dirty" limit where σ can be taken to be $q_{\parallel}$ independent. Another limit where the dependence of σ on $q_{\parallel}$ can be neglected (at least in the nonsuperconducting state) is when $q_{\parallel}\ll k_F$ and $q_{\parallel}v_F/\omega\ll 1$, where v_F is the Fermi velocity. The former condition is almost always satisfied in dipole scattering since $q_{\parallel}\lesssim 0.01$ Å^{-1}. In dipole scattering $q_{\parallel}\sim\omega/v$ the latter condition reduces to $v\gg v_F$. This condition is reasonably well satisfied for the new high-T_c materials owing to the small Fermi velocity (low hole concentration and large effective-hole mass). For a more complete discussion of the $q_{\parallel}$ dependence for a two-dimensional (2D) electron gas, see Ref. 23.

The electric potential inside the medium ($z>0$) is of the form

$$\phi=te^{i\mathbf{q}_{\parallel}\cdot\mathbf{x}_{\parallel}-q_{\parallel}z-i\omega t} ,$$

where

$$t=1-g=\frac{2}{1+\epsilon-4\pi q_{\parallel}\sigma/i\omega} .$$

Note that as $\sigma\to\infty$,

$$t\to-\frac{i\omega}{2\pi q_{\parallel}\sigma} .$$

Hence, for "large" σ the electric field is screened out for $z>0$, and no bulk excitations (e.g., phonons) will occur in the loss spectra.

B. Stacks of conducting 2D layers

This case corresponds to layered materials such as TiS_2 or $YBa_2Cu_3O_7$ if one assumes that the bulk properties remain unchanged right up to the surface and if the surface is terminated by the same conducting layers. For this case it can be shown that

$$g=-\lim_{N\to\infty}\frac{(A^N)_{21}}{(A^N)_{11}} , \tag{5}$$

where A is a 2×2 matrix

$$A=\begin{bmatrix} a_{11} & a_{12} \\ a_{21} & a_{22} \end{bmatrix}$$

with the components

$$\begin{aligned}
a_{11}&=(\epsilon+1)(1+\epsilon-4\pi q_{\parallel}\sigma/i\omega)\\
&\quad+(\epsilon-1)(1-\epsilon-4\pi q_{\parallel}\sigma/i\omega)e^{-2q_{\parallel}d} ,\\
a_{12}&=(\epsilon-1)(1+\epsilon-4\pi q_{\parallel}\sigma/i\omega)\\
&\quad+(\epsilon+1)(1-\epsilon-4\pi q_{\parallel}\sigma/i\omega)e^{-2q_{\parallel}d} ,\\
a_{21}&=(\epsilon+1)(1-\epsilon+4\pi q_{\parallel}\sigma/i\omega)\\
&\quad+(\epsilon-1)(1+\epsilon+4\pi q_{\parallel}\sigma/i\omega)e^{-2q_{\parallel}d} ,\\
a_{22}&=(\epsilon-1)(1-\epsilon+4\pi q_{\parallel}\sigma/i\omega)\\
&\quad+(\epsilon+1)(1+\epsilon+4\pi q_{\parallel}\sigma/i\omega)e^{-2q_{\parallel}d} .
\end{aligned}$$

Two limits of (5) are of particular importance: For "large" σ the electric field from the external electron will be screened out already by the first conducting sheet. From (5) it follows that, as $\sigma\to\infty$,

$$g\to 1+\frac{i\omega}{2\pi q_{\parallel}\sigma} .$$

Hence,

$$\mathrm{Img}\approx\frac{\omega}{2\pi q_{\parallel}}\mathrm{Re}\left[\frac{1}{\sigma}\right]=\frac{\omega\rho}{2\pi q_{\parallel}}=\frac{\omega\rho'}{2\pi q_{\parallel}d} , \tag{6}$$

where ρ is the two-dimensional resistivity (units of Ω) and $\rho'=\rho d$ the three-dimensional resistivity (units of Ω cm) which would result *if* the medium were built up from an infinite sequence of conducting sheets (separation d) with the same properties as the top sheet. (In reality, the actual bulk sheets may, however, have different properties from the top sheet.) From here on we will use the same notation ρ for the two-dimensional and three-dimensional resistivity but the unit (Ω and Ω cm, respectively) defines the relevant quantity. Note that the electric field in the limit of large σ will be nearly orthogonal to the top sheet and that the strength of the electric field just below the first conducting sheet is reduced by a factor

$$\left|\frac{i\omega}{2\pi q_{\parallel}\sigma}\right|\sim\frac{\omega\rho}{2\pi q_{\parallel}}$$

relative to above it. In dipole scattering $q_{\parallel}\sim\omega/v$ so that the condition of "large" σ is effectively $\rho v/2\pi\ll 1$.

Another important limit is as $\sigma\to 0$ (or $\rho v/2\pi\gg 1$). In this case the conducting sheets do not screen well and the electric field will penetrate "deep" (100–1000 Å) into the solid. In this case (5) reduces to

$$g=1-\frac{2}{1+\sqrt{\epsilon_{\parallel}\epsilon_{\perp}}} , \tag{7}$$

where $\epsilon_{\perp}=\epsilon$ and $\epsilon_{\parallel}=\epsilon-4\pi\sigma/di\omega$ are the dielectric functions in the orthogonal and parallel directions, respectively. This formula can also be derived directly from Maxwell's equations for an anisotropic solid described by a dielectric tensor of the form

$$\begin{bmatrix} \epsilon_{\parallel} & 0 & 0 \\ 0 & \epsilon_{\parallel} & 0 \\ 0 & 0 & \epsilon_{\perp} \end{bmatrix} . \tag{8}$$

C. 2D layered material with a modified surface layer

This case corresponds to a layered material as in case (b) but with a modified top layer. As we will see below, modification of the top layer often occurs in real systems. The g function for this case is rather complicated, but for most of the applications in this paper it is not necessary to use this general result.

In the applications to TiS_2 and the $Bi_2Sr_2CaCu_2O_8$ materials presented below, two drastically different regions on the crystal surfaces are observed: "high"-resistivity regions where (7) holds and "low"-resistivity regions where screening is effective and (6) holds. On the other hand, for the $YBa_2Cu_3O_7$ crystals low-resistivity regions are mainly found. Note that in this latter case the HREELS signal is directly proportional to the resistivity ρ of the top layer [see Eq. (6)], a fact that will be used later.

In HREELS one does not measure $P(k,k')$ directly, but rather this quantity integrated over the acceptance angle of the analyzer

$$\Delta P = \int_{\Delta\Omega} d\Omega_{k'} P(k,k') \ .$$

In the present case $\Delta\Omega$ can be taken as a circular aperture centered in the specular direction. The quantity ΔP is obtained from the experimental-loss spectra via $\Delta P = h'/h\Gamma$, where $h\Gamma$ is the area under the elastic peak (h is the "height" and Γ the full width at half maximum) and $h'(\omega)$ is the "height" of the loss background at the loss energy ω. The discussion above assumes that inelastic multiple scattering can be neglected. For the experimental data presented in Fig. 11(c), the inelastic scattering is very strong and in analyzing these data we have accounted for inelastic double scattering.

In order to illustrate the range of validity of approximations (6) and (7), Fig. 4 shows ΔP as a function of the resistivity ρ for a layered system of type 2(b). In this calculation $\Delta\theta = 1°$, the angle of incidence $\alpha = 45°$, the incident electron energy $E_0 = 2.6$ eV, and the loss energy $\hbar\omega = 50$ meV. The conducting sheets are assumed to be separated by 12.3 Å and the dielectric slabs between the conductions sheets are described by the dielectric function $\epsilon = 4$. The solid curve in the figure shows the result of the full calculation using (3) and (5). Note that $\Delta P \to 0$ as $\rho \to 0$ and as $\rho \to \infty$. These results are easy to understand physically as follows: As $\rho \to \infty$, the system moves towards an insulating state where no low-energy excitations can occur. On the other hand, as $\rho \to 0$ the conductivity $\sigma \to \infty$, and, as a result, the effective electric field in the conducting layer will be screened out. The dash-dotted curve in Fig. 4 has been calculated using the "high"-resistivity result (7). As expected, this formula agrees well with the full calculation for $\rho > 2\pi d/v \approx 100\,\mu\Omega$ cm. The dashed curve is the result obtained if the model shown in Fig. 2(a) is used, i.e., for one single conduction sheet on top of a semi-infinite dielectric medium. For $\rho < 2\pi d/v$, this calculation agrees well with the full calculation (solid line) which shows that in this case the electric field is completely screened out beyond the first conducting sheet and ΔP is therefore, according to Eq. (6), directly proportional to the resistivity on the top conducting sheet. Finally, note that for an experimentally given ΔP there are two corresponding solutions for ρ: a "high"-resistivity solution ρ_H and a "low"-resistivity solution ρ_L. For example, if $\Delta P = 10^{-2}$ (eV)$^{-1}$ then $\rho_L = 3\,\mu\Omega$ cm and $\rho_H = 10^7\,\mu\Omega$ cm. Which of these two solutions is correct must be judged from physical reasonableness, e.g., by comparing with other measurements of the resistivity.

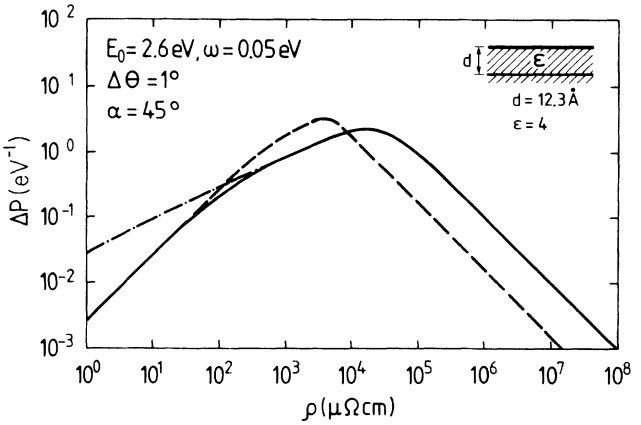

FIG. 4. A model calculation of the EEL signal ΔP for the model indicated in Fig. 2(b). The conducting sheets are characterized by a real and frequency-independent resistivity ρ. The conducting sheets are separated by dielectric slabs (dielectric function $\epsilon = 4$) of thickness $d = 12.3$ Å. The incident electron energy is $E_0 = 2.6$ eV and the loss energy $\hbar\omega = 50$ meV. The analyzer is focused in the specular direction ($\alpha = 45°$) and collects electrons within a space angle (FWHM) $\Delta\theta = 1°$. The solid line is the result of the full calculation using Eqs. (3) and (5). The dashed line is the result obtained from (3) and (4), i.e., assuming only one conducting layer on top of a semi-infinite dielectric medium [see Fig. 3(a)]. The dash-dotted line is calculated using a macroscopic dielectric-function approach [Eqs. (3) and (7)].

Let us comment on the relation between HREELS and light reflection spectroscopy which has been frequently used for the studies of the dielectric properties of layered materials. Consider first a p-polarized light beam incident on the system shown in Fig. 2(a). It is easy to calculate the reflection factor r. For normal incidence ($q_\parallel \to 0$) one gets

$$r = 1 - \frac{2}{1 + \sqrt{\epsilon} + 4\pi\sigma/c} \tag{9}$$

and the transmission factor is given by $1 - r$. Note that the response from the conducting sheet is reduced by a factor $\sim \omega/cq_\parallel$ ($q_\parallel$ is the parallel momentum transfer in dipole scattering) compared with that of dipole scattering [Eq. (4)]. In dipole scattering $q_\parallel \sim \omega/v$ so that this reduction factor amounts to $v/c \approx 1/300$ since $v \approx 10^6$ m/s in the most HREELS measurements. Hence, HREELS is about 300 times more surface sensitive than light reflection spectroscopy. Another important consequence of this strong reduction in the contribution from σ for each layer in an optical measurement is that, when calculating the dielectric response for a layered system [case 2(b)], it is usually not necessary to perform a "mi-

croscopic" calculation involving coupled conducting sheets. One can instead base the derivation on Maxwell's equation for an anisotropic, homogeneous solid characterized by the dielectric tensor of the form (8). For example, for the important case of a light beam incident at a normal angle to the layers (i.e., the electric field vector parallel to the layers), one gets the reflection factor

$$r=1-\frac{2}{1+\sqrt{\epsilon_{\parallel}}} \tag{10}$$

and the reflectance $R=|r|^2$.

The frequency-dependent resistivity $\rho(\omega)$ is perhaps the single most important quantity which can be deduced from HREELS of layered materials. To close this section, let us briefly review how, within the BCS theory, ρ depends on temperature and frequency for a "dirty" superconductor. Again we use "dirty" in the sense that strict $q_{\parallel}$ conservation does not occur. For this case, the conductivity $\sigma(\omega)=\sigma_1(\omega)+i\sigma_2(\omega)$ has been calculated by Mattis and Bardeen.[24] Figure 5(a) shows the result for σ_1 and σ_2 for two temperatures, $T=0.17T_c$ (dashed line) and for $T=0.77T_c$ (solid line). The frequency is measured in units of twice the gap parameter Δ and the conductivity σ_s in the superconducting state in units of the conductivity in the normal state σ_n. Note that the gap parameter Δ is temperature dependent, i.e,, the normalization of the frequency ω by 2Δ in Fig. 5 is different for the two curves. For $T=0$ K, no energy absorption can occur for $\omega<2\Delta$. For $\omega>2\Delta$, energy absorption can occur by splitting a Cooper pair. This process is dipole-forbidden for a clean BCS superconductor but allowed when random scattering centers are introduced. The reduction of symmetry at the surface in addition to surface defects and bulk-derived inhomogeneities are thereby expected to provide the necessary scattering centers which allow us to experimentally observe the superconducting gap. For $T_c>T>0$, energy absorption can occur for all frequencies owing to thermally excited electron-hole pairs. Figure 5(b) shows the result for $\rho=\sigma_1/(\sigma_1^2+\sigma_2^2)$ and in Fig. 5(c) we show

$$\tilde{\rho}=\frac{(\sigma_1^2+\sigma_2^2)^{1/2}-\sigma_2}{\sigma_1^2+\sigma_2^2}$$

in units of $\tilde{\rho}$ in the normal state. As already discussed ρ can be measured by HREELS and, as we will see later, $\tilde{\rho}$ can be determined from IRAS at low frequencies. Obviously, in the BCS theory $\tilde{\rho}(\omega)$ has a similar structure to $\rho(\omega)$ in the gap region. However, the unity crossing and shape of ρ_s/ρ_n more clearly defines a gap than either σ or $\tilde{\rho}$ ratios.

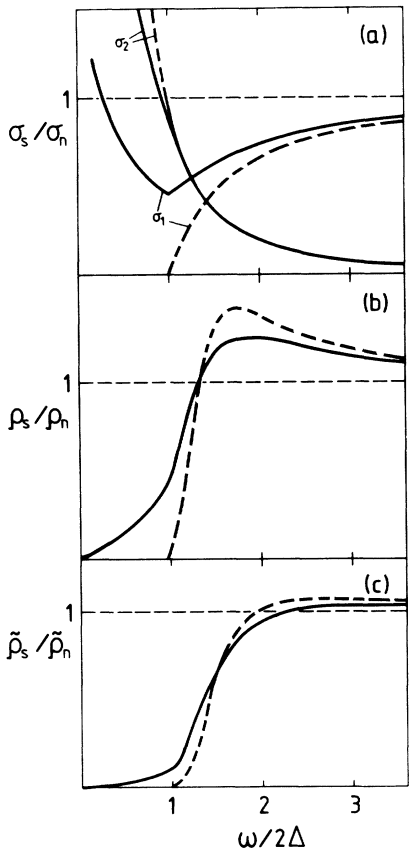

FIG. 5. (a) The Mattis-Bardeen result for the conductivity $\sigma=\sigma_1+i\sigma_2$ as a function of frequency ω for two different temperatures $T/T_c=0.17$ (dashed line) and 0.77 (solid line). (b) The same as (a) but now for the resistivity $\rho=\sigma_1/(\sigma_1^2+\sigma_2^2)$. (c) The same as (a) but now for the quantity $\tilde{\rho}=[(\sigma_1^2+\sigma_2^2)^{1/2}-\sigma_2]/(\sigma_1^2+\sigma_2^2)$.

IV. EXPERIMENTAL RESULTS AND ANALYSIS

In this section we will present and analyze experimental HREELS data from 1:2:3, 2:2:1:2, and TiS_2 crystals. The latter crystal also has a layer-type structure and is included here mainly to demonstrate that other layered crystals, when cleaved, also produce terminations with drastically different transport properties.

A. Cleaved 1:2:3 crystals

Figure 6 shows a series of HREELS spectra from a small flat region of a 1:2:3 crystal cleaved initially at 298 K. A "hump" in the inelastic signal is clearly seen at $\simeq 60$ meV at low temperature. As the temperature increases the "hump" decreases. In order to analyze these spectra we subtract away the tail of the elastic peak (dashed curve in the 22-K data) taken from the gain side of the HREELS spectra. This also removes the Bose-Einstein factor since the intensity on the gain side (beyond the tail of the elastic peak) is $\sim n_{\omega}$ while it is proportional to $n_{\omega}+1$ on the loss side (see discussion in Sec. III). Figure 7 shows the resistivity at $T=22$ K as deduced from another spectra taken for a sample cleaved at $T=22$ K using the theory presented in Sec. III. As pointed out in Sec. III for a given ΔP, there are two solutions for the resistivity and physical arguments must be used to choose the correct solution. In the present case we have rejected the high-resistivity solution as this would give $\rho\sim 10^7$ $\mu\Omega$ cm which is unreasonable (see below). The three curves in the figures are the results obtained assuming different acceptance angles of the spectrometer. The actual acceptance angle was determined to be between $1°<\Delta\theta<1.25°$. Since the resistivity of the top layer is rather small, the first conducting layer will screen

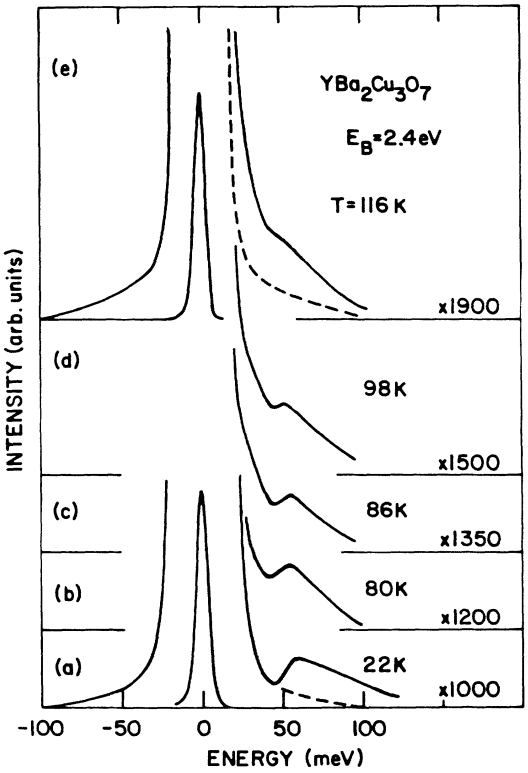

FIG. 6. A sequence of HREEL spectra as a function of temperature from a 1:2:3 crystal cleaned in ultrahigh vacuum. Experimental conditions: $E_0=2.6$ eV, $\alpha=45°$, $\Delta\theta=1°$.

the electric field from the external electrons almost completely so that the electric field will not act on the second and deeper-lying conducting layers. Hence, the resistivity in Fig. 7 refers to the resistivity of the top layer alone, i.e., the *a-b* plane of 1:2:3. The curves in Fig. 6 are similar to the BCS prediction for ρ_s/ρ_n and we will refer to

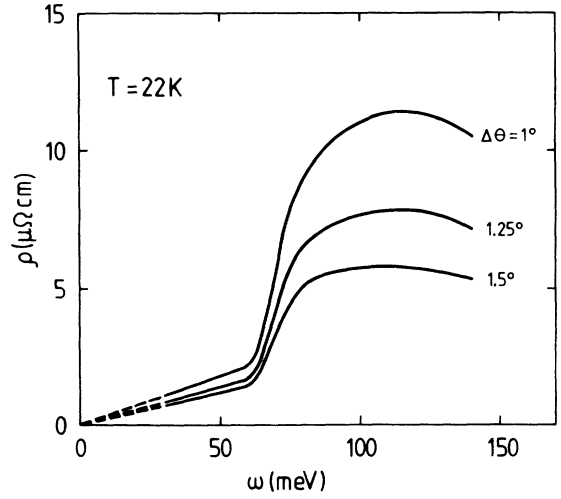

FIG. 7. The frequency-dependent resistivity as deduced from the $T=22$ K spectra in Fig. 6. The result for $\rho(\omega)$ is shown for three different assumed acceptance angles. In the calculation $E_0=2.6$ eV, $\epsilon_0=4$, $\alpha=45°$ (specular scattering), and $d=12.3$ Å.

the "onset" at $\omega\simeq 60$ meV as the gap frequency which would be 2Δ in the BCS theory. However, as we will show later, the temperature dependence of the gap is not that expected from BCS theory. Note also that finite adsorption occurs below the gap frequency which, of course, deviates from the simple BCS theory prediction for $T=0$ K (see Fig. 5). However, some background associated with random or regional inhomogeneities may, in fact, be necessary to allow us to detect the gap. We further note that this background also appears to depend on the cleavage quality and varies from sample to sample. Thus, at least part of this experimental background is most likely the result of surface inhomogeneities. In the gap region we see little evidence for another gap down to 25 meV which is the lowest frequency we can reliably probe due to the energy "tails" of the elastic beam.

As discussed in Sec. III, in the low-resistivity limit the HREELS signal is directly proportional to the resistivity ρ. By taking ratios of the superconducting and normal-state HREELS signals, we can avoid the uncertainties in deriving the resistivity as shown in Fig. 7. In Fig. 8 we show the ratio

$$\Delta P(T)/\Delta P(125\text{ K})=\rho(T)/\rho(125\text{ K})$$

for $T=22$, 80, and 116 K derived from the HREELS measurements shown in Fig. 6. As the temperature increases the gaplike feature at $\hbar\omega\simeq 55$ meV gradually decreases in magnitude but the gap position varies little with temperature. In particular, it does not go to zero as BCS theory predicts.

To elucidate the nature of superconductivity, we plot the ratio of the gap position (obtained from the onset in the loss spectra) relative to its position at 22 K in Fig. 8(b) and compare this to BCS theory[25] (dashed line). The dotted curve labeled H corresponds to the height of the

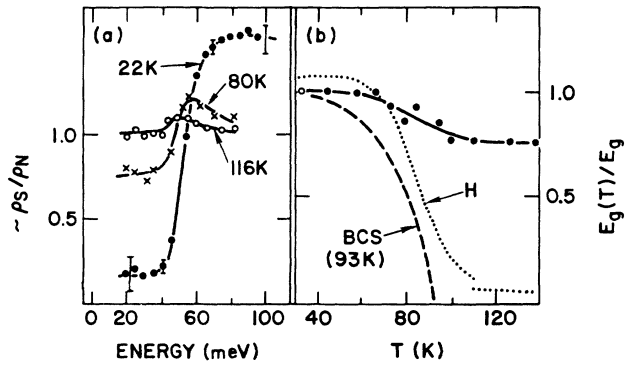

FIG. 8. (a) Ratio of the superconducting loss spectra at different temperatures to the normal-state loss spectra at 125 K showing the evolution of the gap and (b) the evolution of the loss spectra onset with temperature (solid line). The dotted line H shows the height of the superconducting onset in the loss spectra above and below the gap. The discontinuity in H at 116 K arises from the electron beam damage occurring for consecutive scans above T_c. The resistivity below the gap at 22 K varies for the samples studied and is found to depend on cleavage quality and electron beam irradiation above T_c. The data shown here is from our best, i.e., optically flat, cleave.

superconducting onset in the loss spectra. As superconductivity disappears, the gap is reduced but does not follow BCS theory. Even at 80 K the gap shown in Fig. 8(a) is well defined and only weakly shifted. In Table I we summarize the most well-defined gaps we have observed for both 1:2:3 and 2:2:1:2 surfaces, and which we believe are representative of our data on these surfaces. We note that 1:2:3 surfaces irradiated at temperatures above T_c show a shift in the gap to ~ 40 meV for a wide range of exposures. We can associate this with the 60-K T_c plateau for oxygen deficient bulk samples.[26] Alternately, considering the ir measurements discussed next, this may reflect a modified binding energy of the bosons. The average of these experimental results indicates a gap of $(7.8\pm0.3)k_B T_c$.

It is of interest to compare the results obtained above with the recent infrared reflection spectroscopic measurements by Orenstein *et al.*,[7] which reached a different conclusion than the earlier infrared work by Schlesinger and Collins *et al.*[6] In Fig. 9 we reproduce Orenstein's results for the reflectivity as a function of frequency for two different samples with $T_c = 30$ and 90 K. The different T_c's are a result of different sample preparations and are believed to reflect different concentrations of holes in the oxygen p band. As a function of temperature, a sharp decrease in the reflectivity is observed near ~ 60 meV toward low temperatures in all the measured spectra. This actually agrees well with the "gap" position in both our HREELS data as well as the earlier ir data and interpretations.[6] Let us analyze the reflectivity data in more detail in order to directly compare the results with our HREELS data. For $R \geq 0.8$, Eq. (9) reduces to within a good approximation to

$$R = |r|^2 \simeq 1 - 4\,\mathrm{Re}\frac{1}{1+\sqrt{\epsilon_{\parallel}}} ,$$

where $\epsilon_{\parallel} = \epsilon - 4\pi\sigma/id\omega$. If we take $\epsilon = 4$ as above, then for $R \geq 0.8$, we can, to a good approximation, neglect ϵ compared with $4\pi\sigma/id\omega$ giving

$$R \simeq 1 - 4\,\mathrm{Re}\frac{1}{\sqrt{4\pi i\sigma/d\omega}} .$$

TABLE I. Summary of observed gap values for the different Cu-O–based superconductors. Electron irradiation produces a gap that persists over a range of irradiation which we associated with the T_c plateau of 60 K for O-deficient bulk samples.

	T_c (K)	2Δ (meV)	$2\Delta/k_B T_c$
	1:2:3		
RT cleave	93	55	6.8
LT cleave	93	70	8.7
O-deficient	~ 60	40	~ 7.8
	2:2:1:2		
LT cleave	85	58	7.9
LT cleave	91	60	7.6
		Average	7.8 ± 0.3

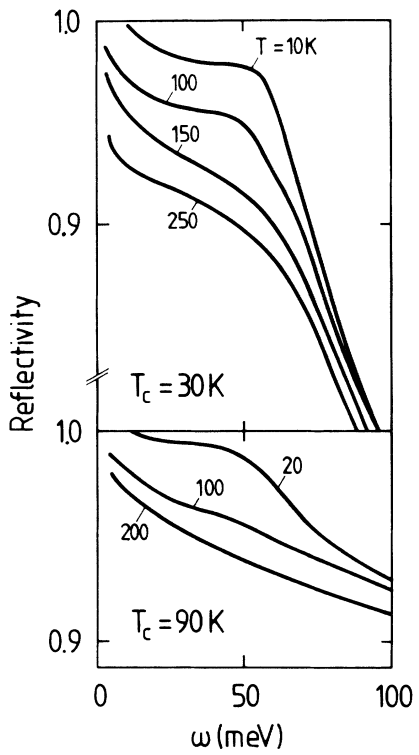

FIG. 9. Reflectivity as a function of frequency from two different 1:2:3 crystals with $T_c = 30$ and 90 K, respectively. Some data from Orenstein *et al.*, Ref. 7.

Writing $\sigma = \sigma_1 + i\sigma_2$ gives

$$R = 1 - \sqrt{2\omega d\tilde{\rho}/\pi} ,$$

where

$$\tilde{\rho} = \frac{(\sigma_1^2+\sigma_2^2)^{1/2} - \sigma_2}{\sigma_1^2+\sigma_2^2} .$$

Figure 10 shows $\tilde{\rho}$ for a variety of crystals with different T_c's which were obtained directly from the reflectivity data in Fig. 9 by Orenstein *et al.*[7] as well as from data by Schlesinger and Collins *et al.*[6] The dashed line in Fig. 10(b) shows $\rho = \sigma_1/(\sigma_1^2+\sigma_2^2)$ as obtained from $\tilde{\rho}$ by (approximately) relating σ_2 to σ_1 via the Ferrell-Glover sum rule as discussed by Tinkham.[27] Figure 10(c) shows $\tilde{\rho}$ for the original results of Schlesinger *et al.*[6] Both infrared results on 1:2:3 for $\tilde{\rho}$ are very similar to that deduced from our HREELS data (see Fig. 7) except that the overall magnitude of the resistivity deduced from the reflectivity data is a factor $\sim 5-10$ larger.

There are two possible explanations for this difference in resistivities which we briefly discuss. In ir spectroscopy the measured resistivity is the average over a distance ~ 1000 Å into the sample, while in the HREELS case, ρ refers to the topmost conducting layer. Hence, if we assume that the top layer has modified properties (resulting in a lower resistivity) as compared with the underlying layers, this would explain the observed results. However, for the superconducting surfaces one expects rather rigid conditions to allow superconductivity. Alternately, the

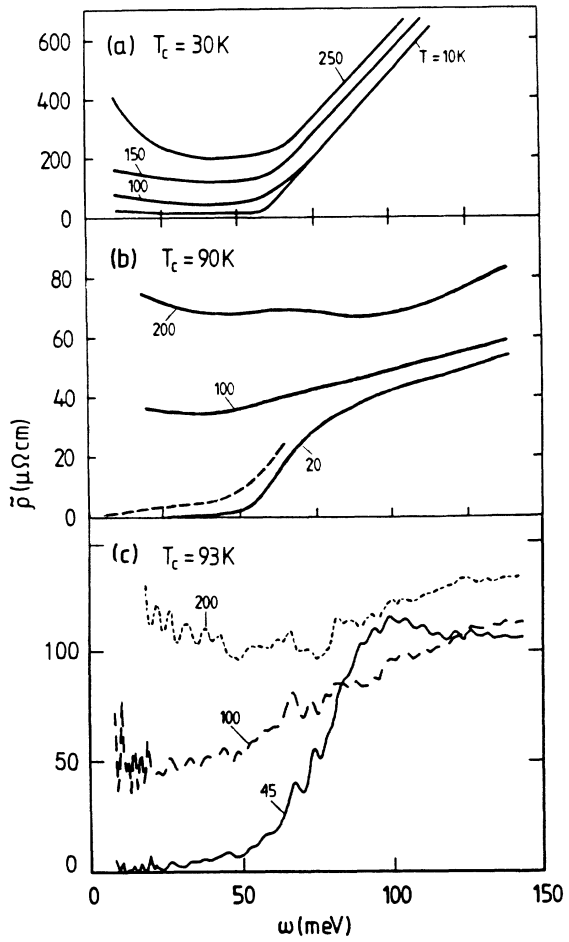

FIG. 10. (a) and (b) show the quantity $\tilde{\rho}$ as deduced from the $T_c = 30$- and 90-K spectra in Fig. 9 from the data by Orenstein *et al.*, Ref. 7. (c) shows $\tilde{\rho}$ from the earlier ir data by Schlesinger and Collins *et al.*, Ref. 6, for a 1:2:3 sample with a T_c of 93 K. The dashed line in (b) is discussed in the text.

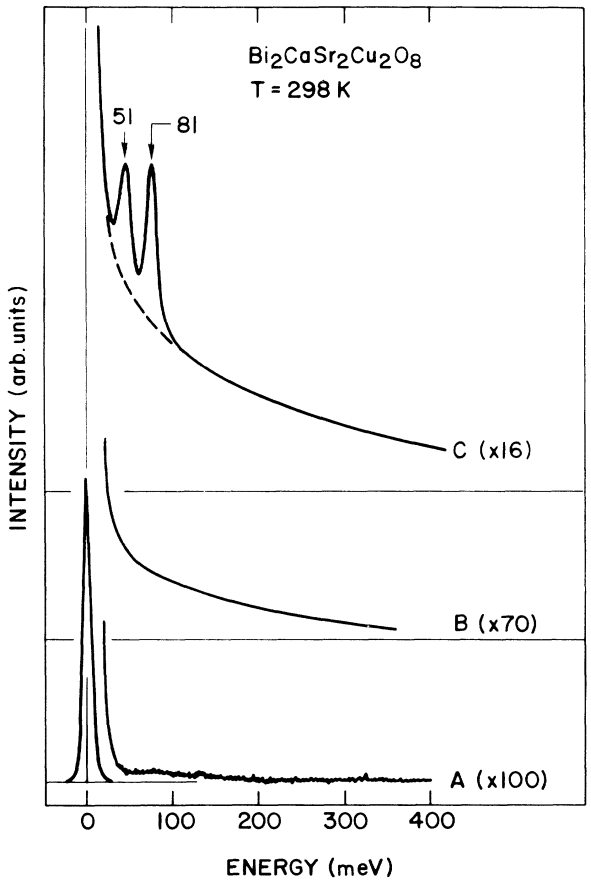

FIG. 11. HREEL spectra from three different regions, $A-C$, on a cleaved 2:2:1:2 crystal.

differences in the lateral coherence length scales of these two probes could result in probing different contributions to ρ. Note that the wavelength of ir light at the loss energy $\omega = 50$ meV is about 0.02 mm while in HREELS the characteristic lateral length scale over which the electric field varies is smaller by a factor of $v/2\pi c \approx 0.001$, where v is the velocity of the electrons. Furthermore, since most ir studies aimed at studying the conductivity in the *ab* plane are performed close to normal incidence, the electric field in the ir case can vary even slower parallel to the surface than determined by the wavelength of the light. For example, in the study by Orenstein *et al.*[7] the angle of incidence is 10° giving a lateral variation lengtl of about 0.14 mm. It is conceivable that given the inhomogeneities we find, HREELS is better able to probe the intrinsic layer resistivity due to its smaller coherence length.

B. Cleaved 2:2:1:2 crystals

Figure 11 shows HREELS spectra from three different regions on a cleaved 2:2:1:2 crystal where regions *A* and *C* occur the most frequently and almost exclusively on our best samples. Note that the loss intensity in region *C* is more than a factor of 100 stronger than on region *A*. As will be shown below, the surface of region *A* has a relative low resistivity ($\rho \sim 30$ μΩ cm) and we will refer to this area as having high conductivity. On the other hand, the region *C* has much higher resistivity ($\gtrsim 1000$ μΩ cm) and we will refer to this area as having low conductivity. Region *B* we attribute to an unidentified metallic intergrowth. On the high-conductivity area the electric field from an incoming electron is screened out by the first conducting sheet (see Sec. III) and no phonon loss is seen in the spectra. On the other hand, for the low-conductivity regions, the electric field penetrates 100–1000 Å into the crystal. In this case we observe two strong phonon losses [Fig. 11c)]. The reason for why a low-conductivity region can have a higher EEL signal than a high-conductivity region was explained in Sec. III (see Fig. 4). We note that the variation of the elastic reflectivity with the kinematic energy E_0 of the electrons is very different for regions *A* and *C* as shown in Ref. 17 and allows us to easily locate these two different regions. As pointed out in Sec. II, we find that these different regions have different reflectivities to polarized light. For example, spectra *C* was found to arise on the darker region shown in Fig. 2(b) and has its polarization rotated

90° relative to the other regions. As discussed earlier, we associate this polarization difference to a switching of the a and b directions of 2:2:1:2. From HREELS this region also appears to have an increased resistivity.

In region C the resistivity is sufficiently high ($\rho \gtrsim 1000\ \mu\Omega$ cm) that we can use (7) in analyzing the HREELS data. We write

$$\epsilon_{\parallel}=\epsilon-\frac{4\pi ne^2/d}{m^*\omega(\omega+i/\tau)} ,$$

$$\epsilon_{\perp}=\epsilon+\sum_{j=1}^{2}\frac{4\pi a_j}{1-\frac{\omega}{\Omega_j}\left[\frac{\omega}{\Omega_j}+i\frac{\Gamma_j}{\Omega_j}\right]} .$$

Note that we have assumed that the two optical photons Ω_1 and Ω_2 have their dynamical dipole moments orthogonal to the conducting sheets. If the dynamical dipole moments were parallel to the conducting sheets then, owing to screening, unphysically large magnitudes of the dynamical dipole moments would be necessary in order to fit the experimental data. In the analysis we have assumed $\omega<1/\tau$. Hence, the last term in $\epsilon_{\parallel}$ will depend on the resistivity $\rho=m^*d/(4\pi ne^2\tau)$. In all calculations we have used $\epsilon=4$ as derived from the ir studies (see Ref. 28). In the case of the 1:2:3 crystals studied above, the analysis does not depend on ϵ because of the large conductivity of the two-dimensional CuO_2 sheets. However, in the present case the results depend slightly on ϵ.

We have fitted the phonon parameters (a_j,Ω_j,Γ_j) and the resistivity $\rho(\omega)$ in order to reproduce the HREELS data in Fig. 11(c). In Fig. 12 we show the result for $\rho(\omega)$. The frequency dependence of ρ could result either from an inhomogeneous carrier concentration in such a way that the local resistivity is higher at the surface than deeper inside the crystal. (Since $q_{\parallel}\sim\omega$ in HREELS, as ω increases, the HREELS probing depth $\sim 1/q_{\parallel}$ decreases.)

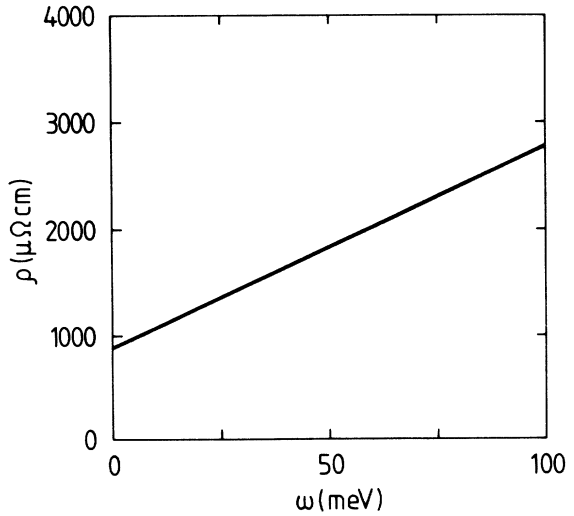

FIG. 12. The frequency-dependent resistivity for region C in Fig. 10.

Alternatively, this frequency dependence of ρ may reflect the intrinsic properties of the crystal in region C. We also note that ρ is weakly temperature dependent, decreasing on average to only 0.7 its room temperature value at 20 K. The optical phonons are described by

$$a_1=0.27,\quad \Omega_1=37\ \text{meV},\quad \Gamma_1=15\ \text{meV} ,$$

$$a_2=0.042,\quad \Omega_2=66\ \text{meV},\quad \Gamma_2=7\ \text{meV} .$$

If we denote the phonon contribution to the polarizability of each unit cell of 2:2:1:2 by $\alpha(\omega)$, then the contribution to $\epsilon_{\perp}(\omega)$ will be $4\pi\alpha/\Delta V$, where ΔV is the volume of the basic unit taken as a rectangular prism with $\Delta V=3.9\times3.9\times15.3=233$ Å^3,

$$\alpha=\sum_{j}\frac{a_j\Delta V}{1-\frac{\omega}{\Omega_j}\left[\frac{\omega}{\Omega_j}+i\frac{\Gamma_j}{\Omega_j}\right]}$$

and we obtain the vibrational polarizabilities $\alpha_1=a_1\Delta V\simeq60.6$ Å^3 and $\alpha_2\simeq9.5$ Å^3. The corresponding dynamic dipole moments are $\mu_1\simeq0.27$ and $\mu_2=0.15\ e$ Å (note: μ_1 is related to α_1 via $\hbar\Omega_1\alpha_1=2\mu_1^2$). Let us now discuss these results in the light of the lattice dynamic calculations by Prade *et al.*[29] These authors have studied the dipole- (and Raman-) active vibrational modes of 2:2:1:2 using the shell model and accounting for both the short-ranged overlap and long-ranged Coulomb potential (but neglecting screening by the free carriers). The parameters in the calculation were taken from fits to the measured phonon dispersion curves of related compounds; the calculated displacement pattern and normal-mode frequencies were estimated to be accurate to within 10%. Six dipole-active modes with the dynamic dipoles orthogonal to the Cu-O planes were found at 17.0, 20.9, 34.3, 41.3, 60.4, and 63.6 meV. Out of these, the first two have too low a frequency to be detected in our measurements. The frequency of the third and fourth mode is very close to the 37-meV peak we observe in the HREELS spectra. Furthermore, since the 37-meV peak is much broader than our experimental resolution we postulate that this peak has contributions from both the $\omega_a=34.2$-meV and the $\omega_b=41.3$-meV mode. Similarly, we believe that the high-frequency peak we observe has contributions from both the $\omega_c=60.4$-meV and the $\omega_d=63.6$-meV mode. However, the frequency of these modes are so close that negligible broadening occurs in the loss spectra in this case. Given that the intensity of a vibrational mode in HREELS is proportional to μ^2 and assuming that this picture is correct, we must reinterpret μ_1 and μ_2 to mean

$$\mu_1^2=\mu_a^2+\mu_b^2,\quad \mu_2^2=\mu_c^2+\mu_d^2 .$$

If one attributes identical effective charges e^* to all the oxygen atoms in 2:2:1:2 then e^* can be calculated (assuming that the effective charge for the other atoms are known) from any one of the two equations given above. We have carried out such an analysis based on the displacement field of the atoms taken from the normal mode

study of Prade *et al.* and find that both the equations above give the same result, $e^* \approx (2 \pm 0.5)e$. This corresponds to the result expected from physical arguments that the oxygen ion is expected to be nearly O^{2-}. This result also provides support of the overall accuracy of our HREELS analysis and our determination of the *ab* layer resistivity. We note that if the vibrational motion were strongly anharmonic or if large charge rearrangements occurred during the vibrational motion, then e^* could be very different from $2e$. For example, a very large dynamical charge of $\sim 6e$ has been observed[30] for the optical Ti-S vibration in the layered compound TiS_2. In this case, accurate electronic structure calculations[31] have indicated that large charge rearrangements occur during the vibrational motion which is the main reason for the large effective charge.

Let us now consider the HREELS spectra from a high-conducting area *A*. Figure 13 shows two such HREELS spectra obtained at two different temperatures, $T=22$ and 298 K. In this case, the conductivity is so high that the electric field is screened out already by the first conducting layer. Hence, the data can be analyzed using (6) and the loss signal is directly proportional to the resistivity of the top layer. The resulting resistivity is shown in Fig. 14. In this case we do not see the same sharp drop in the resistivity at $\omega \sim 50$ meV as for the 1:2:3 materials. However, the quality of this 2:2:1:2 crystal is not as good as the 1:2:3 crystal and later ac susceptibility measurements show a transition width of ~ 20 K. Such inhomogeneities appear to broaden the onset in the loss spectra as well as increase the overall resistivity we find. For instance, our best 2:2:1:2 sample (see Fig. 1, Ref. 17) with $\Delta T_c \sim 3$ K reveals a factor of 3 smaller resistivity. In general, the overall lower quality of the 2:2:1:2 samples and the small amount of superconducting regions we find on these samples have precluded us from measuring the temperature dependence of the gap excitations as done for 1:2:3. It is thereby unclear whether the onset in Fig. 14 is an energy gap of some more insulating

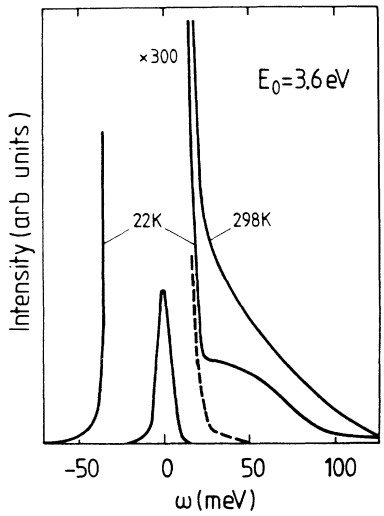

FIG. 13. HREEL spectra at $T=22$ and 298 K from a high-conducting area on a 2:2:1:2 crystal.

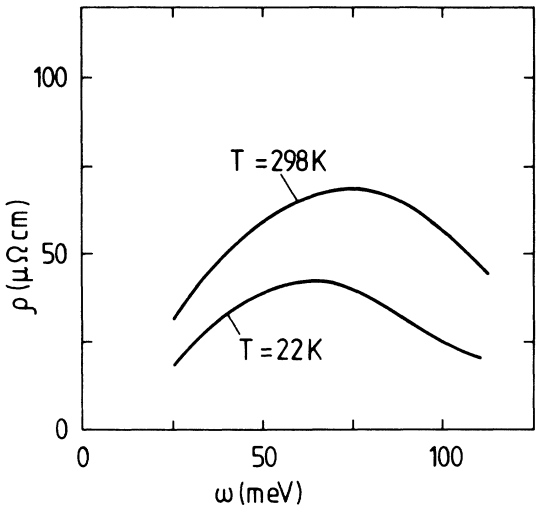

FIG. 14. The frequency-dependent resistivity deduced from Fig. 13. In the analysis we have used $E_0=3.6$ eV, $\Delta\theta=1.65°$, and $\alpha=45°$ (specular scattering).

layers associated with oxygen inhomogeneities, or the excitation energy of the preexisting pairs of a Bose-Einstein condensate.

C. Cleaved TiS_2 crystals

As discussed above, the surfaces of cleaved 1:2:3 and, in particular, 2:2:1:2 crystals exhibit regions with drastically different transport properties. However, this does not appear to be a special property of the high-T_c materials. To illustrate this we show some of our HREELS measurements on cleaved TiS_2 crystals. These crystals consist of stacked TiS_2 planes kept together by weak forces (e.g., Van der Waals forces).[32] The TiS_2 crystal is a small-gap semiconductor, but because of inevitable deviations from stochiometry (extra Ti atoms), the TiS_2 crystal is usually a generately *p*-doped semiconductor. The surface of *in situ* cleaved TiS_2 shown in Fig. 15 exhibits a region of "high" conductivity (a) and other regions of "low" conductivity (b). The HREELS signal from a low-conductivity region is about ~ 100 times larger than for a high-conducting region. The resistivity of a high-conductivity region is approximately temperature and frequency independent ($\rho \simeq 5$ $\mu\Omega$ cm) while the resistivity of the low-conducting areas is strongly frequency and temperature dependent as expected from the bulk transport properties[29] of TiS_2. Note also that while an optical phonon can be resolved in the HREELS data on the low-conducting region, this phonon mode cannot be resolved on a high-conducting region because of screening. This is very similar to the properties of the 2:2:1:2 crystals presented above. We have already noted in Sec. IV B that TiS_2 has a very strong optical phonon with an effective charge of $\sim 6e$. The fact that it does not show up stronger in the loss spectrum arises since it is polarized along the conducting planes and hence very strongly screened even on the low-conducting regions on the TiS_2 surface. The electronic transport properties of TiS_2 in it-

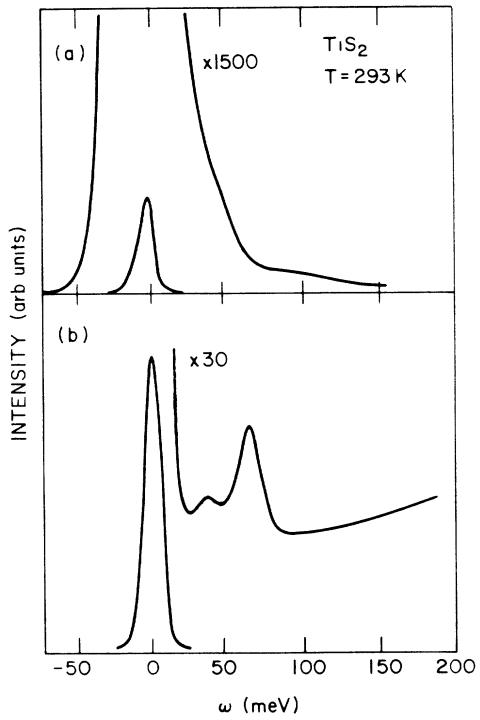

FIG. 15. HREEL spectra from (a) a "high"-conducting area and (b) a "low"-conducting area on a cleaved TiS_2 crystal.

self is a very interesting topic but is not discussed further here.

V. DISCUSSION

In this section, we would like to comment on the gaplike structures we see at $\omega \approx 60$ meV which are the most clearly resolved in the 1:2:3 materials. First of all, it is clear that this structure cannot be explained within BCS theory since the BCS gap $2\Delta \rightarrow 0$ as $T \rightarrow T_c$. In contrast, the gap we observe is almost independent of T. Furthermore, the ir data of Orenstein *et al.*[7] suggests that this gap position does not vary for different values of T_c while, according to the BCS theory, $2\Delta \sim T_c$. One possible explanation is that the gap we observe has nothing directly to do with the superconductivity or pairing, but corresponds to, e.g., an interband transition. However, we consider this explanation unlikely since we see no indication for any other gaplike structures in the $\rho(\omega)$ data. Further very small electron irradiation above T_c dramatically affects this feature as discussed earlier in Sect. VI. Furthermore, if the gap structure were due to an interband transition, one would expect the onset of the transition to depend on the hole concentration (which determines the Fermi-level position) which is not observed in ir. Since the gap structure in $\rho(\omega)$ also occurs for temperatures well above T_c, in particular for the low-T_c samples studied by Orenstein *et al.*, we postulate that the gap energy $\hbar\omega_{\text{gap}} \approx 60$ meV corresponds to the pairing energy, i.e., the energy where two holes pair to form a boson with charge $2|e|$. The superconductivity transition at T_c is then interpreted as a Bose-Einstein condensation of preexisting pairs. Of course, we do not consider this transition to be a pure Bose-Einstein transition but to be somewhere between the BCS limit (where $2\Delta \approx 3.5 k_B T_c$) and the ideal Bose-Einstein condensation limit, where the gap (here defined as the energy necessary to split a boson into its fermion components) is independent of T_c.

Recently,[3,4] several photoemission studies of $Bi_2Sr_2CaCu_2O_2$ ($T_c = 90$K) have been reported. For $T < T_c$ the photoemission intensity as a function of energy develops a structure close to the Fermi energy suggesting the opening up of a gap with $\Delta \approx 30 \pm 5$ meV, i.e., $2\Delta / k_B T = 8 \pm 1.4$, in good agreement with our results for Y-Ba-Cu-O. This is a further strong indication that the "hump" we see at 60 meV is related to superconductivity and not due to an interband transition, since such a transition would not show up in the photoemission spectra at all. It is also interesting to note that Manzke *et al.*[4] find that, in some of their temperature runs, they were able to observe temperature effects starting well above T_c. This is consistent with our HREELS data which show that the "hump" disappears above T_c. We have also observed a temperature-dependent gap on one area of a 1:2:3 cleaved surface that suggests a superconducting phase with an estimated T_c of 120 K.

An alternative important method to measure the gap 2Δ is by nuclear magnetic resonance (NMR) spectroscopy.[33] Several such measurements were recently performed on Y-Ba-Cu-O. The anisotropy of the gap parameter $\Delta(k)$ in k space complicates the analysis of these data and a simple activated behavior such as $1/T_1 \sim \exp(-\Delta / k_B T)$ expected for an isotropic BCS-type superconductor is infrequently observed. If the data nevertheless is interpreted in this way, a gap of $2\Delta \approx (6-8) k_B T_c$ is usually obtained which is similar to that we have found. Even in the normal state $1/T_1$ does not behave "normal." There seems to be highly correlated motion of the electrons and the electron spins in this type of material which is picked up by the nuclear spins. These deviations from the prediction of the BCS theory are consistent with the behavior deduced above for the "gap".

Another standard method to measure the gap is by tunneling. For a long time tunneling measurements gave irreproducible results which depended on, e.g., the way the tunneling junction was prepared.[2] Recently, reproducible measurements have been performed by Geerk *et al.*[34] that indicate a large gap. These authors prepared sandwich-type tunneling junctions of the 1:2:3 material, where the barrier consisted of a thin layer of insulating 1:2:3 material. These tunneling junctions give $2\Delta \approx 60$ meV. However, a finite tunneling density of states appears in the "gap" even for tunneling at low temperature. Again, it is unclear whether this background is intrinsic or reflects inhomogeneities, such as metallic regions, associated with stronger hole doping or modified surface layers associated with forming the tunnel barrier. In these studies a naturally grown oxide barrier was also used,[33] again giving reproducible results but with $2\Delta \simeq 40$ meV. Interestingly, this agrees with the smaller gap we obtain for electron radiated 1:2:3 and which we associate

with the 60-K T_c plateau for oxygen-deficient samples.[26]

From a theoretical point of view, it is not surprising if the BCS theory fails to describe the high-T_c materials. It has been repeatedly pointed[35] out that since the coherence length in the conducting planes ξ (the size of a Cooper pair) is exceptionally short[36] (about 10 Å in Y-Ba-Cu-O) and the density of (hole) carriers $n = l^{-2}$ relatively low, the condition $l \approx \xi$ is satisfied. The BCS theory, being a mean-field theory, is valid only if $\xi \gg l$. For $\xi \ll l$ it is better to think of preexisting or "real-space" pairs formed at some higher temperature rather than in the weak-coupling limit at T_c. In this alternative picture, superconductivity would simply be a consequence of Bose-Einstein condensation of preexisting pairs. For a quasi-two-dimensional ideal Bose gas (e.g., a set of stacked weakly coupled planes containing the bosons), the Bose-Einstein condensation temperature[37] $T_c \sim n$ and this relation seems to hold for the high-T_c materials. Emery has suggested that the same relation $T_c \sim n$ is also expected from weak-coupling (BCS) theory if the excitation giving rise to pairing (Cooper pair formation) has an energy larger than the Fermi energy E_F. In this case, $T_c \sim E_F \sim n$ since $E_F \sim n$ for a two-dimensional electronic system. However, we can now rule out this suggestion since the temperature dependence of the gap Δ is not in accordance with the prediction of weak-coupling (BCS) theory.

An often raised objection against a model based on a Bose-Einstein condensation of preexisting pairs has been that the transition temperature deduced from such a model is believed to be much too high (see, e.g., Ref. 35). But, as is well known, for a strict two-dimensional system $T_c = 0$, and it is only because of the weak interlayer coupling that $T_c > 0$. For a quasi-two-dimensional system with a low concentration n^* of bosons and for $m_\parallel / m_\perp \ll 1$, one has[36]

$$k_B T_c \approx \frac{2\pi n^* \hbar^2}{m_\parallel \ln(2 k_B T_c m_\perp d^2/\hbar^2)} , \tag{11}$$

where $m_\parallel$ and $m_\perp$ are the effective mass of a boson in the $\parallel$ and $\perp$ directions, respectively, and d is the layer separation. Taking reasonable numbers $m_\parallel = 10$ m, $m_\perp = 100$ m (where m is the electron mass), $d = 12.3$ Å, and $n^* = 0.01$ Å^{-2} gives $T_c \approx 200$ K which is in the range of the observed transition temperatures. Nevertheless, we do not believe that the simple model on which Eq. (11) is based is accurate or complete enough to quantitatively describe the transition. The point we wish to make, however, is that there is no *a priori* reason to exclude the possibility of having a Bose-Einstein condensation with T_c as low as 90 K.

It has been found that the dc resistivity in the high-T_c compounds increases linearly with the temperature up to at least $T \approx 500$ K (see Ref. 12). If $E_{\text{gap}} \approx 60$ meV is the Cooper pair binding energy and if the pairs exist even above T_c as suggested above, this would lead to a problem in understanding the linear temperature dependence of the dc resistivity. The point is that, at $T = 500$ K, one could expect a non-negligible fraction of the pairs to have thermally been broken up into its fermion components. However, if the dc conductivity is due to the Cooper pairs plus free fermions at high temperatures, but only Cooper pairs at low temperatures, there would be no reason to expect a linear temperature dependence in the temperature interval $T \lesssim 500$ K.

As noted earlier, we find markedly smaller frequency-dependent resistivities for the superconducting and normal state of these materials then found by ir as well as other macroscopic resistivity measurements. Given the small length scale that HREELS probes, in addition to the degree of surface inhomogeneities we find, as well as the sensitivity of superconductivity to doping or surface changes, we believe these low resistivities are, in fact, intrinsic to superconductivity in the *ab* plane. As noted earlier, even some HREELS derived resistivities on 2:2:1:2 were found to be larger on samples which showed severely broadened superconducting gaps, i.e., where inhomogeneities clearly exist.

VI. SUMMARY AND CONCLUSIONS

In this work we have presented electron-energy-loss data from two high-T_c materials, namely 1:2:3 and 2:2:1:2 and also from TiS_2. These data were analyzed using the dipole-scatter theory. The main conclusions can be summarized as follows.

(1) On the surfaces of all the cleaved crystals, and in particular 2:2:1:2 and TiS_2, we find areas with drastically different conductivities. In the high-conductivity terminations of all three layered materials studied, the first conducting layer screens out the electric field of the incoming electrons and the loss spectrum is then directly proportional to the resistivity ρ of this top layer.

(2) The frequency dependence of $\rho(\omega)$ for 1:2:3 at low temperature exhibits a "gap"-like feature at $\omega = 60$ meV. Small residual absorption in the gap is found which likely occurs from inhomogeneities of the top layer that are not superconducting. As the temperature increases, the "jump" in the resistivity at the gap decreases continuously with little change in the gap position.

(3) The infrared reflectivity data on single crystals by two groups[6,7] for 1:2:3 samples showing T_c's = 90 K gives very similar results to those we find. However, the ir measurements[7] for crystals with lower T_c also show gap-like features at $\omega \approx 60$ meV, which persist to even higher temperatures than for the $T_c = 90$-K crystal.

(4) The behavior of the "gap" as a function of temperature and hole concentration (as reflected in the T_c) cannot be explained by BCS theory and we have argued that it is much more in line with a Bose-Einstein condensation of preexisting pairs.

(5) We find significantly higher-conducting layers on both oxide crystals studied compared to both dc and higher-frequency (ir) conductivity measurements of the bulk layers. This is true even for superconducting surface layers and suggests that macroscopic resistivity measurements may be dominated by extrinsic irregularities and imperfection of these layered materials.

Finally, it is important that more HREELS studies of high-T_c materials be performed, in particular, to test

whether, in fact, that what we observe is a "true" gap and that no lower-energy gaps exist beyond the range of the present experiments. The highest resolution of our spectrometer (~ 7 meV) together with our spectrometer background make it difficult to directly see a second gap below 25 meV. However, one of our measurements where exceptional focusing conditions were achieved shows some evidence of another gaplike feature near 22 meV. This result, however, was from a stepped cleaved surface and not reproduced on other samples. A recent review of tunneling results by Kirtley[2] suggests that such smaller gaps reflect tunneling orthogonal to the *ab* plane. Nevertheless, HREELS spectrometers have recently been developed[38–40] with a resolution of ~ 1 meV and, at least in two cases,[39,40] have the possibility to focus the electron beam down to an ~ 100-μm spot diameter. Such HREELS measurements could turn out to be the ideal probe of the superconducting gap structures and layer conductivity of such high-T_c materials.

ACKNOWLEDGMENTS

We would like to thank A. Baratoff, T. Schneider, and J. Kirtley for useful discussions and critical comments on this paper. Discussions with R. Collins, Z. Schlesinger, F. Holtzberg, C. V. Chandrashekhar, C. Tsuei, D. M. Newns, P. M. Horn, S. von Molnár, T. Penney, M. Shafer, F. Himpsel, C. J. Chen, and A. Malozemoff are also acknowledged. For the additional characterization of the samples by micro-Raman, ac susceptibility, and Auger microprobe measurements we thank F. Dacol, C. Feild, R. Schad, and J. Clabes. The laboratory assistance of W. A. Thompson, R. Figat, and J. Schell-Sorokin is also acknowledged.

[1] J. G. Bednorz and K. A. Muller, Z. Phys. B **64**, 189 (1986); J. G. Bednorz, M. Takashige, and K. A. Muller, Europhys, Lett. **3**, 379 (1987); M. K. Wu, J. Ashburn, C. J. Torng, P. H. Hor, R. L. Meng, L. Gao, Z. J. Huang, Y. Q. Wang, and C. W. Chu, Phys. Rev. Lett. **58**, 908 (1987).

[2] J. R. Kirtley, Int. J. Mod. Phys. **4**, 201 (1990); J. C. Phillips, *Physics of High T_c Superconductors* (Academic, New York, 1989), pp. 238–250.

[3] J. M. Imer, F. Patthey, B. Dardel, W. D. Schneider, Y. Baer, Y. Petro, and A. Zettl, Phys. Rev. Lett. **62**, 336 (1989).

[4] R. Manzke, T. Buslaps, R. Claessen, and J. Fink, Europhys. Lett. **9**, 477 (1989).

[5] W. Drube, F. J. Himpsel, G. V. Chandrashekhar, and M. W. Shafer, Phys. Rev. B **39**, 7328 (1989).

[6] Z. Schlesinger, R. T. Collins, D. L. Kaiser, and F. Holtzberg, Phys. Rev. Lett. **59**, 1958 (1987); R. T. Collins, Z. Schlesinger, F. Holtzberg, and C. Feild, *ibid.* **63**, 422 (1989).

[7] J. Orenstein, G. A. Thomas, A. J. Millis, S. L. Cooper, D. H. Rapkine, T. Timusk, L. F. Schneemeyer and J. V. Waszczak, Phys. Rev. Lett. **61**, 1313 (1988), and Phys. Rev. B **42**, 6342 (1990).

[8] T. Timusk, S. L. Herr, K. Kamaras, C. D. Porter, D. B. Tanner, D. A. Bonn, J. D. Garrett, C. V. Stager, J. E. Greedan, and M. Reedyk, Phys. Rev. B **38**, 6683 (1988).

[9] F. Slakey, S. L. Cooper, M. V. Klein, J. P. Rice, and D. M. Ginsberg, Phys. Rev. B **39**, 2781 (1989); S. L. Cooper, M. V. Klein, B. G. Pazol, J. P. Rice, and D. M. Ginsberg, *ibid.* **37**, 5920 (1988).

[10] H. Ibach and D. L. Mills, *Electron Energy Loss Spectroscopy and Surface Vibrations* (Academic, New York, 1982).

[11] S. Andersson and B. N. J. Persson, Phys. Rev. Lett. **50**, 2028 (1983); B. N. J. Persson and E. Zaremba, Phys. Rev. B **31**, 1863 (1985).

[12] B. N. J. Persson and J. E. Demuth, Phys. Rev. B **31**, 1856 (1985).

[13] T. Penney, S. von Molnar, D. Kaiser, F. Holtzberg, and A. W. Kleinsasser, Phys. Rev. B **38**, 2918 (1988).

[14] Y. Fukuda, M. Nagoshi, T. Suzuki, Y. Namba, Y. Syono, and M. Tuchiki, Phys. Rev. B **39**, 2760 (1989).

[15] K. Jacobi, D. D. Sharma, P. Geng, C. T. Simmons, and G. Kaindl, Phys. Rev. B **38**, 863 (1988).

[16] M. K. Kelly, Y. Meng, Y. Hwn, Y. Chang, Y. Chen, G. J. Lapeyre, and G. Margaritondo, Phys. Rev. B **40**, 11 309 (1989).

[17] J. E. Demuth, B. N. J. Persson, F. Holtzberg, and C. V. Chandrasekhar, Phys. Rev. Lett. **64**, 603 (1990).

[18] D. L. Kaiser, F. Holtzberg, B. A. Scott, and T. R. McGuire, Appl. Phys. Lett. **52**, 1040 (1987).

[19] G. V. Chandrashekhar, P. Strobel, M. V. Shafer, and F. Holtzberg (unpublished).

[20] B. N. J. Persson and J. E. Demuth, Phys. Rev. B **30**, 5968 (1984).

[21] B. N. Persson and A. Baratoff, Phys. Rev. B **38**, 9616 (1988).

[22] S. R. Streight and D. L. Mills, Phys. Rev. B **35**, 6337 (1987); P. H. Lambin, J. P. Vigneron, A. A. Lucas, P. A. Thiry, M. Liehr, J. J. Pireaux, R. Candano, and T. J. Kuech, Phys. Rev. Lett. **56**, 1842 (1986).

[23] B. N. J. Persson, Solid State Commun. **52**, 811 (1984).

[24] D. C. Mattis and J. Bardeen, Phys. Rev. **111**, 412 (1958).

[25] J. Bardeen, L. N. Cooper, and J. R. Schrieffer, Phys. Rev. **106**, 162 (1957); **108**, 1175 (1957).

[26] R. J. Cava, B. Batlogg, C. H. Chen, E. A. Rietman, S. M. Zahurak, and D. Werder, Phys. Rev. B **36**, 5719 (1987).

[27] M. Tinkham, in *Documents on Superconductivity Modern Physics*, edited by E. W. Montroll, G. H. Vineyard, and M. Levy (Gordon and Breach, New York, 1965).

[28] M. Bauer, I. B. Ferreira, L. Genzel, M. Cardona, P. Murugaraj, and J. Maier, Solid State Commun. **72**, 551 (1989).

[29] J. Prade, A. D. Kulkarni, F. W. de Wette, U. Schroder, and W. Kress, Phys. Rev. B **39**, 2771 (1989).

[30] P. C. Klipstein and R. H. Friend, J. Phys. C **17**, 2713 (1984); G. Lucovsky, W. Y. Liang, and R. M. White, Solid State Commun. **19**, 303 (1976).

[31] A. Zunger and A. J. Freeman, Phys. Rev. B **16**, 906 (1977).

[32] G. K. Wertheim, F. J. DiSalvo, and D. N. E. Buchanan, Solid State Commun. **13**, 1225 (1973).

[33] P. C. Hammel, M. Takigawa, R. H. Heffner, Z. Fisk, and K. C. Ott, Phys. Rev. Lett. **63**, 1992 (1989).

[34] J. Geerk, G. Linker, O. Meyer, Q. Li, R.-L. Wanng, and X. X. Xi, Proceedings of the International M^2S-HTSC Conference, Stanford, 1989, edited by N. E. Phillips, R. N. Shelton,

and W. A. Harrison [Physica C **162-164**, (1989)].
[35]Y. J. Uemura *et al.*, Phys. Rev. B **38**, 909 (1988).
[36]See, e.g., V. J. Emery, IBM J. Res. Dev. **33**, 246 (1989).
[37]R. Micnas, J. Ranninger, and S. Robaszkiewicz, Rev. Mod. Phys. **62**, 113 (1990).
[38]B. Voigtländer, D. Bruckmann, S. Lehwald, and H. Ibach, Surf. Sci. **225**, 151 (1990).
[39]S. Andersson (private communication).
[40]J. Erskine (private communication).

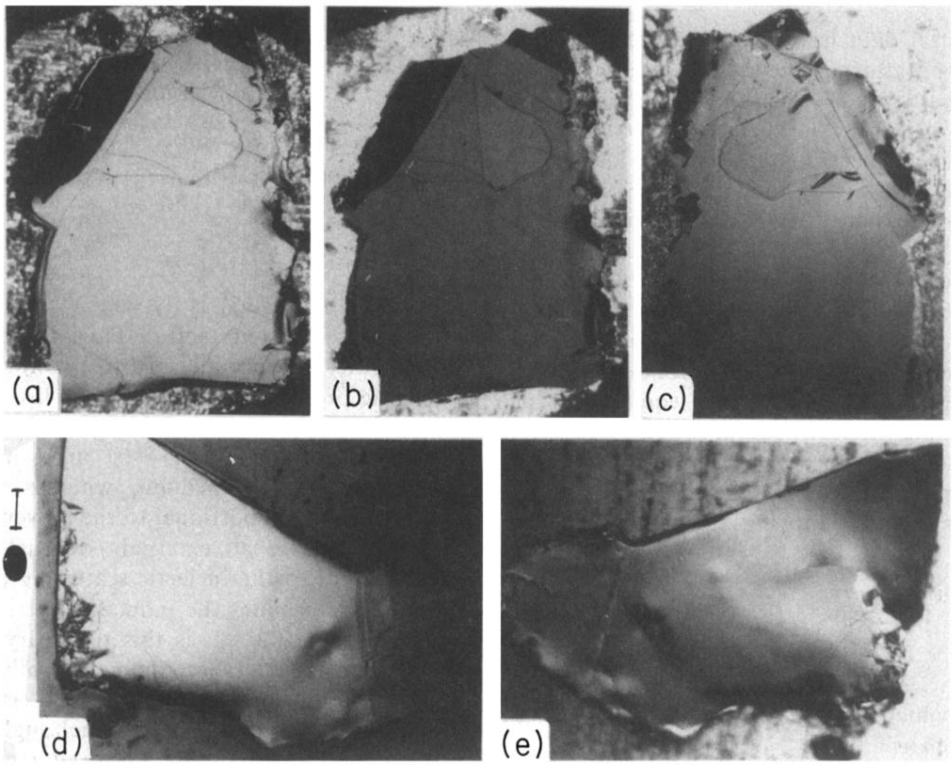

FIG. 2. Micrographs of 2:2:1:2 surfaces under (a) normal light and (b)–(e) polarized light. (b) and (c) and (d) and (e) reflect opposite cleavage pairs of the same sample cleaved in vacuum and in air, respectively. The bar alongside (d) corresponds to 100 μm with the ellipse indicating the beam profile on the sample.